Article

A New Algorithm to Estimate Diffuse Attenuation Coefficient from Secchi Disk Depth

Alejandra Castillo-Ramírez [1,2], Eduardo Santamaría-del-Ángel [1,*],
Adriana González-Silvera [1], Robert Frouin [3], María-Teresa Sebastiá-Frasquet [4], Jing Tan [3],
Jorge Lopez-Calderon [1], Laura Sánchez-Velasco [5] and Luis Enríquez-Paredes [1]

1   Facultad de Ciencias Marinas, Universidad Autónoma de Baja California, Ensenada 22860, Baja California,
    Mexico; alejandra.castillo@uabc.edu.mx (A.C.-R.); adriana.gonzalez@uabc.edu.mx (A.G.-S.);
    jorge.lopez67@uabc.edu.mx (J.L.-C.); lmenriquez@uabc.edu.mx (L.E.-P.)
2   Alumni PhD postgraduate program in Coastal Oceanography, Facultad de Ciencias Marinas,
    Universidad Autónoma de Baja California, Ensenada 22860, Baja California, Mexico
3   Scripps Institution of Oceanography, University of California San Diego, La Jolla, CA 92037, USA;
    rfrouin@ucsd.edu (R.F.); jit079@ucsd.edu (J.T.)
4   Institut d'Investigació per a la Gestió Integrada de Zones Costaneres (IGIC),
    Universitat Politècnica de València (UPV), 46730 Grau de Gandia, Spain; mtsebastia@hma.upv.es
5   Departamento de Plancton y Ecología Marina, Instituto Politécnico Nacional, Centro Interdisciplinario de
    Ciencias Marinas (IPN-CICIMAR), La Paz 23096, Baja California Sur, Mexico; lsvelasc@gmail.com
*   Correspondence: santamaria@uabc.edu.mx

check for
updates

Abstract: The vertical diffuse attenuation coefficient K_d (PAR) is used for calculating the euphotic zone, the first optical depth that is important for primary productivity models. Currently, K_d (PAR) can be estimated using an irradiometer or a Secchi disk (SD). The main objective of this work is to define a model that can be applied to a wide range of optical marine conditions to estimate K_d (PAR) by SD. We used irradiance profiles and SD depth (Z_{SD}) from 679 stations in various marine regions. Three parametric models were developed, and their statistical performance was evaluated in view of previous approaches reported and remote sensing data. The best results were obtained with an adaptive model representing three cases: clear-water, turbid-water, and a transition zone ($R^2 = 0.965$, MAE = 0.083, RMSD = 0.239, BIAS = 0.01, and MPI = 0.854). Previous models considering a single optical depth figure at which the SD disappears did not capture the marine optical complexity. Our classification of 113 stations with spectral absorption data into Jerlov water types indicated that no unique correspondence existed between estimated K_d (PAR) and water type, making it ambiguous to associate compatible inherent optical properties and chlorophyll with Z_{SD}. Although obtaining K_d (PAR) from Z_{SD} is simple/low-cost, care should be taken in the methodology used to measure Z_{SD} to ensure consistent results across different optical marine conditions.

Keywords: Secchi disk; vertical diffuse attenuation coefficient K_d; Secchi disk optical depth; adaptive model; Secchi disk monitoring approach

1. Introduction

Sunlight in the electromagnetic spectrum region between 400 and 700 nm, known as photosynthetically active radiation (PAR) [1], plays an important role in the physics, biology, and chemistry of the oceans [2]. PAR is directly linked to biological processes such as photosynthesis, which constitutes the base of the food chain in marine ecosystems [1,3–5]. In other words, primary productivity largely depends on the sunlight field in the water column, which decreases exponentially with depth.

In the late 19th century, Pietro Angelo Secchi (1866) [6] pioneered studies on the field of light penetration in water and developed a method for determining water transparency based on a white disk (made of a non-refractive material) 30201350 cm in diameter, now known as Secchi disk (SD) [7]. The principle for the use of the SD consists of determining the depth at which it is no longer visible to the naked eye [8]. This depth is defined as the Secchi disk depth (Z_{SD}), being inversely proportional to the amount of dissolved or particulate matter present in the water column; therefore, the Z_{SD} reading can be used as an indicator of turbidity [9,10].

During the 20th century, it was possible to quantify the light field in water, noting that light decreases exponentially with depth. This decrease can be measured using the vertical spectral diffuse attenuation coefficient (K_d), an apparent optical property (AOP) [11] that reflects the attenuation caused by water molecules [12] and the amount and type of compounds in water (phytoplankton, organic and inorganic particles, and colored dissolved organic matter (CDOM)) [13].

Since primary productivity, which controls the evolution of marine ecosystems, largely depends on the sunlight environment in the water column, knowing K_d is essential to describe its variability. For instance, K_d can be used for calculating the depth of the euphotic zone (Z_{eu}) (i.e., the depth at which 99% of the surface light is attenuated) and the first optical depth (qualitatively, the ocean layer that produces the color signal of the ocean recorded by satellites) [1]. K_d is also important for primary productivity models, which are based on the potential of the phytoplankton community to react to different light intensities [14].

K_d can be estimated directly, using irradiance sensors measuring the flow of PAR photons in the water column (K_d(PAR)) [1], or indirectly, using a SD [7]. The former provides more accurate data; however, is not routinely used in oceanographic cruises due to its high cost, but only in those focused on bio-optical measurements or primary productivity, or for the calibration of ocean color sensors [9,15–18]. On the other hand, SD is routinely used in most oceanographic cruises [18–22]. The approximation most commonly used is that K_d(PAR) is inversely proportional to Z_{SD} [9] (Equation (1)), which yields empirical constants. Considering the criteria of Kirk [1] and Gallegos et al. [23], these empirical constants represent the optical depth (OD_{SD}) at which the Secchi disk disappears:

$$K_d(PAR) \; = \; \frac{OD_{SD}}{Z_{SD}}$$

(1)

Poole and Atkins (1929) [9] were the first to propose an OD_{SD} value from 14 measurements recorded in the English Channel, with Z_{SD} values ranging from 2 to 35 m. These authors proposed estimating K_d(PAR) with an OD_{SD} of 1.70. In 1970, at a time when technological progress made it possible to manufacture submersible photometers/irradiance-meters, Holmes [15] revisited this topic; using data from 13 stations in Santa Barbara (California, USA), he derived a value of 1.44. However, the data used by Holmes [15] came from an area with Z_{SD} values ranging from 2 to 12 m, i.e., conditions that were more turbid than those reported by Poole and Atkins [9]. The above studies support using an OD_{SD} of 1.70 for clear water and 1.44 for turbid water (v.gr. Barbosa and Domingues, 2009 [22]).

The above values (i.e., 1.70 and 1.44) were estimated from a limited dataset (14 and 13 stations), which is why several researchers have subsequently sought to re-evaluate these values. Megard and Berman (1989) [16] recorded 24 measurements in the southeastern Mediterranean Sea and estimated an average value of 1.54 for areas with Z_{SD} ranging from 6 to 46 m.

In the marine environment, K_d (PAR) has been estimated from Z_{SD} using OD_{SD} values ranging from 1.22 to 1.70 [22]. Recently, according to the new Secchi Disk Theory [23] and the approach proposed in the Fifth IOCCG Report [24], Lee et al. (2018) [18] proposed to unify all OD_{SD} values into a single figure. These authors used the Hydrolight computer code [25] to simulate the light field in the water column under different optical conditions (from oligotrophic to eutrophic, oceanic and coastal, including phytoplankton blooms). These simulations yielded an average OD_{SD} of 1.48.

Another approach used to estimate K_d (PAR) through SD without involving OD_{SD} involves the development of empirical models based on a nonlinear relationship between K_d(PAR) and $1/Z_{SD}$:

$$K_d(PAR) \ = \ \frac{a}{(Z_{SD})^b} \tag{2}$$

where a and b are the empirical coefficients of the model, which vary according to the study area. The majority of the work on models given by Equation (2) has been conducted for inland water bodies [26–28]. For marine environments, Montes-Hugo and Alvarez-Borrego [17] proposed values of 1.45 and 1.10 for a and b, respectively, for coastal waters in the northeast of Baja California and southern California, an area with Z_{SD} from 2 to 12 m.

Jerlov [29] classified oceanic water into five types (I, IA, IB, II, and III) and coastal water into five types (1, 3, 5, 7, and 9), based on hyperspectral K_d (K_d (λ)) for each wavelength), where a larger number indicates higher turbidity. Each of the 10 Jerlov water types has a typical light absorption coefficient associated ($a(\lambda)_{model}$) [30]. This absorption coefficient takes into account pure sea water absorption, $a_w(\lambda)$, chlorophyll-based absorption, $a_{phy}(\lambda)$, and CDOM absorption, $a_{CDOM}(\lambda)$ [30] (Equation (3)):

$$a(\lambda)_{model} \ = \ a_w(\lambda) + a_{phy}(\lambda) + a_{CDOM}(\lambda) \tag{3}$$

where λ is wavelength.

Based on the above, estimating K_d (PAR) from Z_{SD} measurements has proven to be a useful, cost-effective methodology to detect changes in marine ecosystems. However, it is essential that the K_d (PAR) estimates be robust and objective, since a miscalculation of K_d(PAR) would lead to errors in estimates of euphotic zone and first optical depths. The main objective of this work is to establish an empirical relationship that could be applied to a wide range of optical conditions occurring in marine environments. A second objective is to examine whether the K_d(PAR) derived from Z_{SD} could be related to a specific optical water type (in Jerlov's sense), which would broaden the application of the SD approach and enhance its usefulness as a descriptor of water optical properties. Likewise, and considering that the current development of spectroradiometer-type remote sensors allows producing synoptic measurements of K_d at 490 nm (K_d(490)), this study considered data from these remote sensors as one of the models to evaluate.

2. Materials and Methods

In this study, we compiled 679 pairs of K_d (PAR) and Z_{SD} data recorded under well-illuminated (sunny) conditions, with an irradiance meter and SD, respectively. These encompass conditions from clear oceanic to turbid coastal waters (Figure 1a,b). The source of data was as follows: 212 data pairs from the Tara Ocean Consortium [31] (Figure 1a); 195 from the NASA SeaBass archive (Chesapeake bay and CALCOFI zone) [32]; 103 from Gallegos et al. [21]; 74 from the Phytoplankton Ecology Group (POPEYE) database at Universidad Autónoma de Baja California; 71 from Montes-Hugo and Alvarez-Borrego [17]; 24 from Megard and Berman [16]. Hereafter, K_d(PAR) recorded from irradiance-meter data will be named $K_{d\,in\,situ}$.
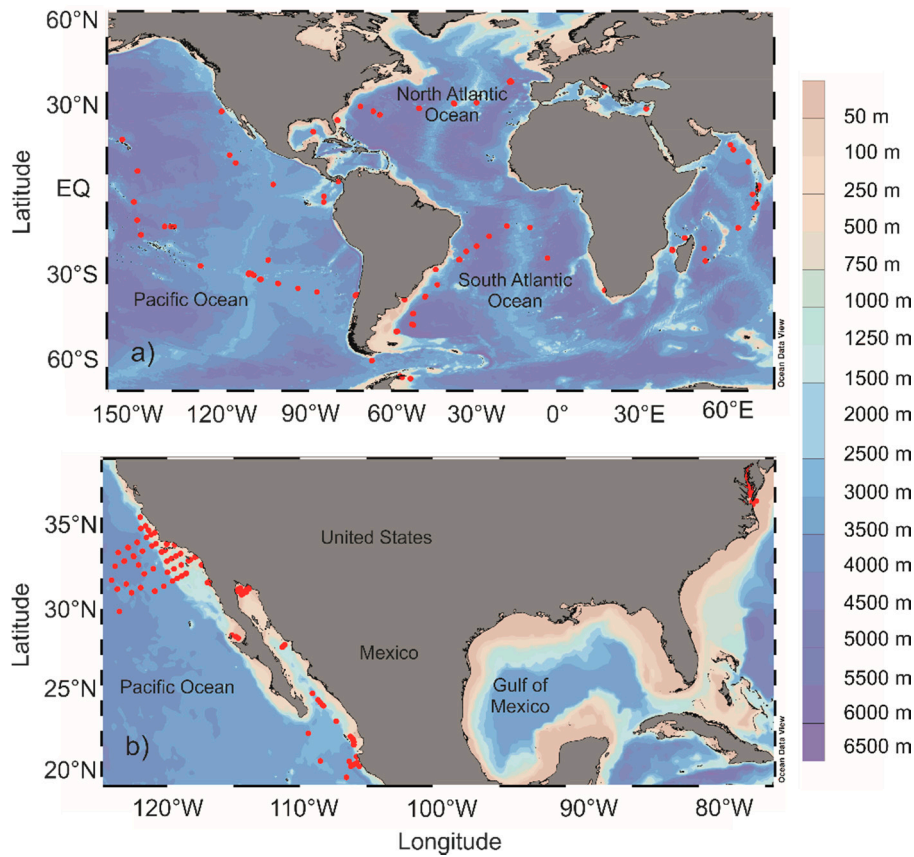
Figure 1. Location of stations; the color bar indicates the bathymetry, in meters. (**a**) Stations of the Tara Ocean Stations Consortium [31] and Megard and Berman [16]. (**b**) Stations of the NASA SeaBass file [32], POPEYE database, Gallegos et al. [21], and Montes-Hugo and Alvarez-Borrego [17].

$K_{din\ situ}$ for NASA SeaBass [32] and POPEYE data was estimated for each station based on PAR measurements, in accordance with the criteria of Kirk [1], expressed in Equation (4):

$$ln(PAR(Z)) = ln(PAR(0)) - K_{din\ situ}\ Z \tag{4}$$

where $K_{din\ situ}$ is the slope of a linear model and the dependent variable is the natural logarithm of irradiance as a function of depth (Z). For the Tara Ocean Consortium data [31], $K_{din\ situ}$ was estimated from Z_{eu} using the following equation [1]:

$$Z_{eu} = \frac{4.6}{K_{din\ situ}} \tag{5}$$

The $K_{din\ situ}$ data of Megard and Berman [16], Montes-Hugo and Alvarez-Borrego [17], and Gallegos et al. [21] were taken from those reported in the respective publications.

Based on Steyerberg [33] and the IOCCG report [34], the database was randomly split into two groups. Group 1 was used for the development of models; it comprises 478 data pairs (70% of total data). Group 2 was used for validation purposes; it comprises 201 data pairs (30% of total data). To reduce the random error in the selection of the two datasets and to test the robustness of models, 10 replicates were obtained by randomly selecting 10 different datasets for modeling, along with the respective validation datasets.

Three parametric models were tested to predict K_d (PAR) based on Z_{SD}; the model with the best fit was selected as per the criteria of Xu et al. [35] for least-squares analysis. The first approximation (model *a*) was based on Equation (1), where K_d (PAR) is calculated using fixed (or single) estimates of

OD_{SD}; the second (model *b*) was based on the nonlinear empirical relationship between $K_{din\ situ}$ and $\frac{1}{Z}_{SD}$ (Equation (2)); and the third (model *c*) followed the concepts of Equation (2); in the latter model, Z_{SD} was split into three zones, namely two extreme cases (clear and turbid waters) and a transition zone, as follows:

$$log_{10}(K_d) \ = \ p1 + p2 \times log_{10}(Z_{SD}), \text{ if } log_{10}(Z_{SD}) < p3 \tag{6}$$

$$log_{10}(K_d) \ = \ p5 + p6 \times log_{10}(Z_{SD}) \text{ if } log_{10}(Z_{SD}) \geq p4 \tag{7}$$

In the transition zone, where $p3 \leq log_{10}(Z_{SD}) < p4$, $log_{10}(K_d)$ is modeled as a linear combination of the two models:

$$log_{10}(K_d) \ = \ (p1 + p2 \times log_{10}(Z_{SD})) \times \frac{p4 - log_{10}(Z_{SD})}{p4 - p3} + (p5 + p6 \times log_{10}(Z_{SD})) \times \frac{log_{10}(Z_{SD}) - p3}{p4 - p3} \tag{8}$$

The model parameters p1, p2, p3, p4, p5, and p6 are retrieved through the least-squares fitting.

Moreover, K_d (490) values were derived from measurements with a 1 × 1 km-resolution spectroradiometer in monthly multi-sensor composites. The sensors used were Ocean Color and Temperature Scanner from August 1996 to July 1997 (OCTS_v2014.0), Sea-Viewing Wide Field-of-View Sensor (SeaWiFS) from September 1997 to December 2010 (SeaWiFS_v2018.0), Moderate Resolution Imaging Spectroradiometer-MODIS TERRA from February 2000 to date (MODIST_v2018.0), Medium Resolution Imaging Spectrometer (MERIS) from April 2002 to March 2012 (MERIS_R3), Moderate Resolution Imaging Spectroradiometer-MODIS-AQUA from July 2002 to date (MODISA_v2018.0), and Visible and Infrared Imager/Radiometer Suit (VIIRS) Suomi-NPP from January 2012 to date (VIIRS_v2018.0). Sensor data to construct these images were downloaded from [36] to 1B level and processed at levels 2 and 3 using SeaDAS 7.5.1. (National Aeronautics and Space Administration) The multi-sensor composites were performed following the criteria by [37,38].

To determine the performance from the above models, three statistical descriptors were calculated: mean absolute error (MAE) (Equation (9)), root-mean-square error (RMSD) (Equation (10)), and analysis of bias (BIAS) (Equation (11)).

$$MAE \ = \ \frac{\sum \left| (K_{din\ situ} - K_{dmodel}) \right|}{n} \tag{9}$$

$$RMSD \ = \ \sqrt{\frac{\sum (K_{din\ situ} - K_{dmodel})^2}{n}} \tag{10}$$

where *n* is the total number of data included in this analysis, $K_{din\ situ} - K_{dmodel}$ is residual observations, and $\left| (K_{din\ situ} - K_{dmodel}) \right|$ is the absolute value of residuals.

$$BIAS \ = \ average \ (K_{din\ situ} - K_{dmodel}) \tag{11}$$

where *BIAS* is the residual mean.

According to MAE and RMSD, lower values represent better results, whereas BIAS values closer to zero mean better results. To determine which is the best model, a model performance index (MPI) was estimated (Equation (12)) based on the three statistic descriptors mentioned above:

$$MPI \ = \ 1 - \left(\frac{\left(\frac{R_{MAE}}{p} \right) + \left(\frac{R_{RMSD}}{p} \right) + \left(\frac{R_{|BIAS|}}{p} \right)}{3} \right) \tag{12}$$

where R_{MAE} is the MAE rank, R_{RMSD} is the RMSD rank, $R_{|BIAS|}$ is the rank of absolute BIAS values, and *p* is the total number of models to be compared. Ranks and their respective matches were calculated following the criteria of [39–41]. MPI ranges from 0 to 1, where values closer to 1 mean a better model.

To accomplish the objective of examine whether the K_d (PAR) derived from Z_{SD} could be related to a specific optical water type (in Jerlov's sense), we compiled in-situ absorption coefficient data

$(a(\lambda)_{in\ situ})$. These were available for 113 stations only. The data for the POPEYE database and the CALCOFI zone were processed following the protocol of Mitchell et al. [42], whereas the data for the Chesapeake Bay area were analyzed following the protocol of Mueller and Austin [43]. Pope and Fry [12]) values were used for $a_w(\lambda)$. $a(\lambda)_{in\ situ}$ spectra were classified into the different Jerlov water types. The classification was obtained by comparing $a(\lambda)_{in\ situ}$ with $a(\lambda)_{model}$ using a least-squares fitting method based on Xu et al. [35]. The statistical significance of this fit was determined through a goodness-of-fit test following Zar [44]. POPEYE absorption data ranged from 400 to 700 nm, and SeaBaSS data from 400 to 650 mm. Thus, the goodness-of-fit test was carried out with different degrees of freedom, according to each dataset (POPEYE: $\alpha = 0.05$, $\chi^2_{Crit} = 21.02$, df = 12; SeaBASS: $\alpha = 0.05$, $\chi^2_{Crit} = 18.30$, df = 10).

3. Results and Discussion

Our database includes both oceanic and coastal stations (Figure 1), so the models presented in this work were developed and evaluated considering a wide range of optical conditions. The three models proposed in this work represent $K_{d\,in\ situ}$ and Z_{SD} values ranging from 0.030 to 3.217 m^{-1}. and 0.3 to 50 m, respectively.

Model a based on Equation (1) and that gives rise to Equation (13) yielded an OD_{SD} of 1.37 ($R^2 = 0.957$), which is lower than OD_{SD} values reported in the literature. Typically, studies performed in the 20th century considered that low OD_{SD} values resulted from increased turbidity [13,45]. However, the authors of [18] mentioned that in addition to the above, a factor to consider is that when K_d (PAR) is estimated using shallow depths, this tends to be higher than values estimated for deeper layers. This trend is most evident in oceanic stations with deeper Z_{eu} relative to stations where light penetration is lower. In other words, lower OD_{SD} values may be obtained when the calculation of K_d (PAR) considers the light profile from the surface to a depth close to Z_{eu}, or at least to Z_{SD} [18]. In determining OD_{SD}, $K_{d\,in\ situ}$ was calculated using light profiles close to Z_{eu} or Z_{SD}.

$$K_{d\,model\ a} = \frac{1.37}{Z_{SD}} \tag{13}$$

Model b was based on a nonlinear fit between $K_{d\,in\ situ}$ and Z_{SD}, (Equation (14)), assuming that this represents the continuous function of the empirical relationship between K_d (PAR) and Z_{SD}. This model resulted in regression coefficients $a = 1.18$ and $b = 0.92$ ($R^2 = 0.957$). These coefficients are lower relative to those reported by Montes-Hugo and Álvarez-Borrego [17] ($a = 1.45$ and $b = 1.10$), likely because of the narrower sampling interval (1–12 m) used by these authors.

$$K_{d\,model\ b} = \frac{1.18}{(Z_{SD})^{0.92}} \tag{14}$$

Model c is adaptive and followed the same approach as model b, i.e., it comprises three equations that consider three Z_{SD} ranges (Equations (15)–(17)) ($R^2 = 0.965$). These Z_{SD} ranges represent two contrasting conditions: turbid water with $Z_{SD} < 2.20$ m (Equation (15)) and clear water with $Z_{SD} \geq 5.37$ m (Equation (17)); plus a transition zone with 2.20 m $\leq Z_{SD} < 5.37$ m (Equation (16)).

$$K_{d\,model\ c} = \frac{1.16}{(Z_{SD})^{0.62}} \tag{15}$$

$$K_{d\,model\ c} = \exp\left((0.15 - logZ_{SD} \times 0.62) \times \tfrac{1.68 - logZ_{SD}}{0.89} + (-0.48 - logZ_{SD} \times 0.72) \times \tfrac{logZ_{SD} - 0.79}{0.89}\right) \tag{16}$$

$$K_{d\,model\ c} = \frac{0.62}{(Z_{SD})^{0.72}} \tag{17}$$

The equation for the transition zone (Equation (16)) is more complex since attempting to discern stations located between these two extremes (turbid-to-clear vs. clear-to-turbid stations), while keeping

continuity in Z_{SD} over the entire Z_{SD} range. This partitioning into Z_{SD} ranges in the model c allowed us to reduce variability in the data, i.e., achieve a better fit for each case, therefore providing better performance overall.

For evaluating models a, b, and c, $K_{d\ in\ situ}$ (Equations (4) and (5)) was compared versus $K_{d\ model\ a}$ (Equation (13)), $K_{d\ model\ b}$ (Equation (14)), and $K_{d\ model\ c}$ (Equations (15)–(17)) (Figure 2), as well as versus K_d estimated from the different models for marine waters reported in the literature (Table 1). These comparisons were evaluated based on MAE (Equation (9)), RMSD (Equation (10)), BIAS (Equation (11)), and MPI (Equation (12)). The above showed that model c (Figure 2c) yielded the best fit (lowest MAE, RMSD, BIAS close to zero, and MPI closest to one), MAE of 0.083, RMSD of 0.239, BIAS of 0.01, and MPI of 0.854.
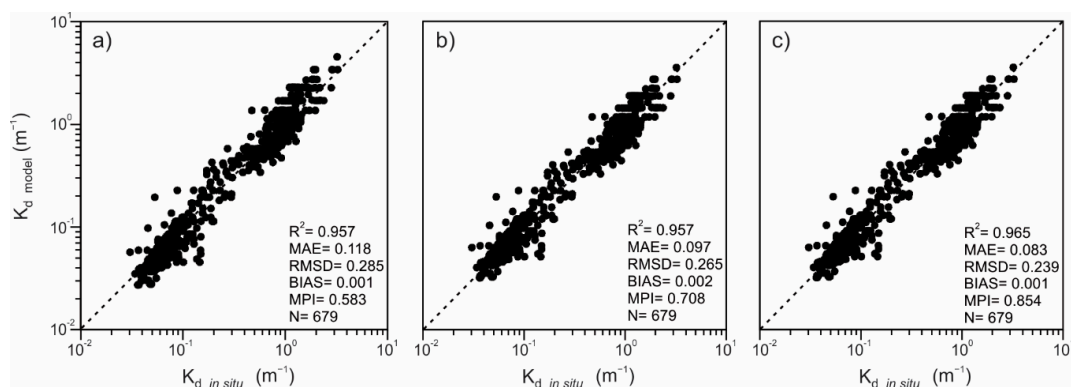
Figure 2. Comparative analysis between the attenuation coefficient estimated in situ ($K_{d\ in\ situ}$) and the attenuation coefficients modeled. (**a**) $K_{d\ model\ a}$, (**b**) $K_{d\ model\ b}$, and (**c**) $K_{d\ model\ c}$.

Table 1. Evaluation of $K_{d\ in\ situ}$ versus Z_{SD} models.

Reference	Equation	Z_{SD} Intervals (m)	MAE	RMSD	BIAS	MPI
Poole and Atkins [9]	$K_d = 1.7/Z_{SD}$	1.9–35	0.182	0.285	0.217	0.104
Poole and Atkins [9]	$K_d = 1.7/Z_{SD}$	1.9–35	0.125	0.273	0.120	0.416
Holmes [15]	$K_d = 1.4/Z_{SD}$	2–12				
Megard and Berman [16]	$K_d = 1.54/Z_{SD}$	6–46	0.142	0.285	0.118	0.229
Lee et al. [18]	$K_d = 1.48/Z_{SD}$	All intervals	0.134	0.285	0.078	0.354
Montes-Hugo and Álvarez-Borrego [17]	$K_d = 1.45/(Z_{SD})^{1.10}$	1–12	0.141	0.359	−0.013	0.250
Model a	$K_d = 1.37/Z_{SD}$	All intervals	0.118	0.285	0.003	0.583
Model b	$K_d = 1.18/(Z_{SD})^{0.92}$	All intervals	0.097	0.265	0.002	0.708
Model c	Equations (15)–(17)	<2.20 Transition zone ≥5.37	0.083	0.239	0.001	0.854

Table 1 represents an improvement versus previous methods, showing that model c yields the best performance considering the statistical descriptors and the index mentioned above. In particular, with respect to the most recent model [18], model c yields a MAE reduction of 0.051, an RMSD reduction of 0.046, and a MPI increase of 0.5.

If models developed for particular or regional marine conditions are considered, such as the model of Lugo-Fernández et al. [46], which divide their conditions for use into summer and non-summer for the north Gulf of Mexico an area influenced by the Mississippi river mouth, highly dispersed results may be obtained as this area is affected by high inland CDOM inputs. Additionally, we consider that the conditions in this model depend on river flows rather than seasonality. Given that our database includes stations from both northern and southern hemispheres, the criteria for applying this model become complex. As an example, we assessed the model of Montes-Hugo and Álvarez-Borrego [17], which was developed only for coastal waters in northeast Baja California and southern California; we observed that the application of this model to different marine conditions yields suboptimal results,

thus highlighting the constraints in generalizing empirical models that were originally established from a limited range of conditions.

The evaluation of models *a* and *b* revealed that the use of a single OD_{SD} value [9,15,16,18] for different optical conditions of water resulted in higher RMSD (Table 1), relative to using two values, i.e., the 1.70 figure proposed by Poole and Atkins [9] for clear waters and the 1.44 figure estimated by Holmes [15] for turbid waters. If we consider the broad range of optical conditions that occur in the marine environment, the above confirms that a single value is certainly not representative of the range of optical conditions. In addition, it was noted that model *b* yields lower RMSD values relative to OD_{SD}.

The three equations adequately represented the range of optical diversity in marine environments (from clear ocean waters to very turbid coastal waters) in a simplified way, and the model can be used even under conditions of phytoplankton blooms such as those described in Santamaria-del-Angel et al. [47] and Aguilar-Maldonado et al. [48].

In order to estimate $K_d(490)$ values from remote sensors for comparison versus $K_{d\,in\,situ}$ and K_d figures estimated with the models in Table 1, 1 km-resolution multi-sensor images were constructed. From the original 679 data, only 383 were used for this comparison. Table 2 evidences that model *c* is the best model, yielding an MPI of 0.814, whereas the models with the worst fit to $K_{d\,in\,situ}$ were the model of Pooole and Atkins [9] and the satellite model, with an MPI of 0.074. To note, the model of [9] was derived from only 14 data that are not representative of the range of optical conditions in the ocean.

Table 2. Evaluation of $K_{d\,in\,situ}$ versus Z_{SD} and satellite models.

| Reference	Equation	Z_{SD} Intervals (m)	MAE	RMSD	BIAS	MPI
Poole and Atkins [9]	$K_d = 1.7/Z_{SD}$	1.9–35	0.041	0.073	−0.028	0.074
Poole and Atkins [9]	$K_d = 1.7/Z_{SD}$	1.9–35	0.034	0.063	−0.006	0.460
Holmes [15]	$K_d = 1.4/Z_{SD}$	2–12				
Megard and Berman [16]	$K_d = 1.54/Z_{SD}$	6–46	0.032	0.063	−0.011	0.425
Lee et al. [18]	$K_d = 1.48/Z_{SD}$	All intervals	0.031	0.062	−0.005	0.740
Montes-Hugo and Álvarez-Borrego [17]	$K_d = 1.45/(Z_{SD})^{1.10}$	1–12	0.034	0.003	0.021	0.425
Model *a*	$K_d = 1.37/Z_{SD}$	All intervals	0.029	0.063	0.007	0.592
Model *b*	$K_d = 1.18/(Z_{SD})^{0.92}$	All intervals	0.032	0.072	0.009	0.388
Model *c*	Equations (15)–(17)	<2.20	0.026	0.062	0.005	0.814
$K_{d\,\textbf{satellite model}}$ (490)	Standard SeaDAS product	Transition zone ≥5.37	0.079	0.187	0.015	0.074

For its part, the satellite model represents K_d (490), which is a spectral portion of the K_d(PAR) measured in situ. Austin and Petzoid [49] proposed the first approach of K_d (490) using the ratio between leaving-water radiances (Lwr) between 443 and 550 nm (Lwr443/Lwr550), as well as the K_d (490) for optically pure seawater and some linear approximation coefficients. A number of approaches have been developed from there, such as those of [32], which essentially have yielded improved estimates of the coefficients used, being specific to each sensor.

Additionally, several authors have estimated Z_{SD} from satellite images, mostly focusing on inland water bodies [50–54]. In the marine environment, Kim et al. [55] estimated Z_{SD} from K_d (490) based on concepts derived from [56–58]. All these point to the need to measure other intrinsic optical properties, such as backscattering at least at 490 nm. As this work did not have in-situ backscattering observations available, we might think that these could be estimated through standard models such as the Generalized Inherent Optical Property (GIOP) model; however, Betancur-Turizo et al. [59] warn that care should be taken with these models because, by being too simplified, they do not reflect the variability of the parameter in a reliable way. This cautionary statement has been addressed recently. The works by Jiang et al. [60] and Liu et al. [61] have aimed to improve these estimates to obtain more accurate satellite Z_{SD} values for various types of water. It is clear that this is a dynamic and constantly evolving line of research.

Although data derived from satellite observations are promising and this subject of research needs to be further refined in the future, we recommend further monitoring of marine optical properties while observing the data quality, and complementing in-situ reflectance measurements.

Based on the above and following the criteria established by [62], the use of multi-sensor data will allow us, in the long term, an improved integration of in-situ measurements and satellite images. This will result in time series that will be suitable for use in marine monitoring programs, defining weekly, monthly, seasonal, and annual variability scales, as well as their trends.

Figure 3 compares $K_{din\ situ}$ and K_{dmodel} calculated using model c and the model of Lee et al. [18]. The results show that both models performed similarly for $K_{din\ situ}$ values lower than 0.1 m^{-1} (clear waters). In more optically complex waters ($K_d > 2$ m^{-1}), the difference between in-situ and modelled data increases. The model of Lee et al. [18] tends to fit a positive exponential (J-shaped) function departing from the 1:1 line, while model c is a closer fit to the 1:1 line. This is evident for the full database (679 observations) and for two independent cruises with different optical conditions (Cal9709: oceanic/coastal conditions; Ties9802: estuarine conditions).
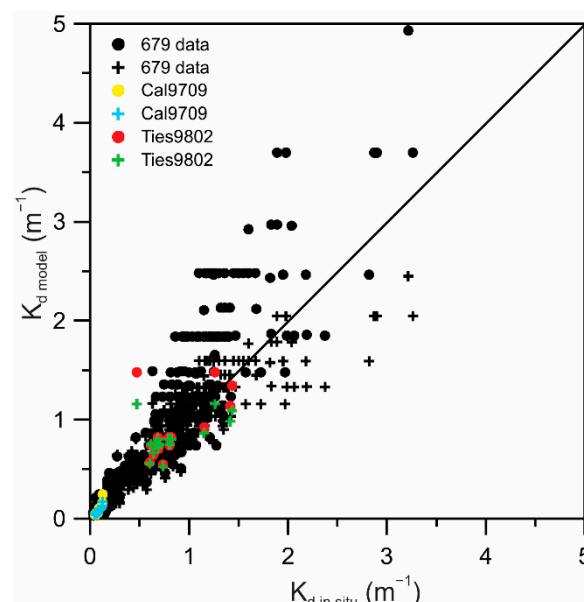
Figure 3. Comparison of $K_{din\ situ}$ vs. $K_{d\ model}$ calculated with the model of Lee et al. [18] (circles) and with model c (crosses), for the full database (black) and for two cruises with different optical conditions: Cal9709 (yellow and blue); Ties9802 (red and green).

The primary objective of this work is to define a model applicable to a wide range of optical conditions in marine environments. Under this premise, model c in an adaptive model that yields better predictions relative to models that consider an OD_{SD} value only. In order to use this model in field cruises, a table was added as supplementary material for $K_d\ (PAR)$ (Table S1), derived from this model and based on Z_{SD}. The most accurate estimate of $K_d\ (PAR)$ with model c allows obtaining better results in the calculation of primary productivity, which is a major variable that can be used in studies ranging from understanding the global carbon cycle to fisheries aspects [63]. A proper understanding of primary organic production will not only allow estimating the total organic matter produced in the oceans, but also supports the comparison of ocean regions as potential food sources [14].

Figure 4a shows K_d values associated with the three Z_{SD} ranges. The clear water case, i.e., $Z_{SD} \geq$ 5.37 m, corresponds to $K_{din\ situ}$ values of less than 0.2 m^{-1} (blue circles); the turbid water case, i.e., $Z_{SD} <$ 2.20 m, to $K_{din\ situ}$ values above 0.4 m^{-1} (brown circles); and the transition zone, to intermediate $K_{din\ situ}$ values. In general, $K_d\ (PAR)$ is inversely related to Z_{SD} [1,9], but with a variable dependence according to the Z_{SD} range, a behavior due to the differential influence of the components that contribute to light attenuation as Z_{SD} change [21].
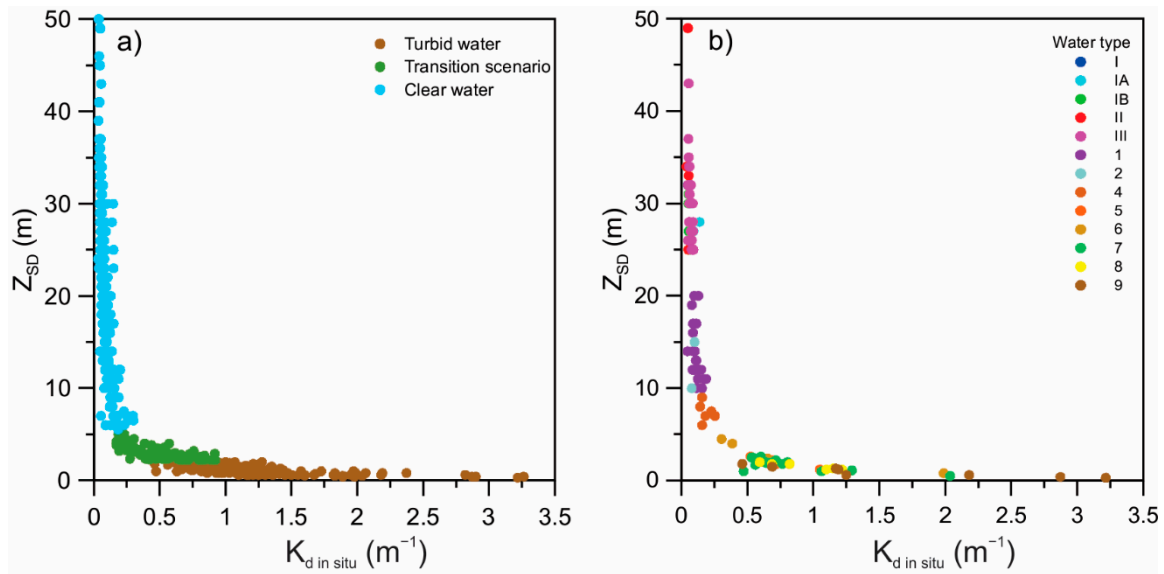
Figure 4. (**a**) Relationship between Z_{SD} and $K_{d\ in\ situ}$ according to three Z_{SD} ranges (679 stations); (**b**) relationship between Z_{SD} and $K_{d\ in\ situ}$ according to Jerlov water type (113 stations with absorption data).

The analysis of $a(\lambda)_{in\ situ}$ resulted in 92 stations classified into a Jerlov water type; the remaining 21 stations failed to meet the criteria for inclusion into a given water type. Intermediate water types were therefore added, i.e., 2, 4, 6, and 8 (Figure 5), supporting the allocation of a water type to the 113 $a(\lambda)_{in\ situ}$ spectra.
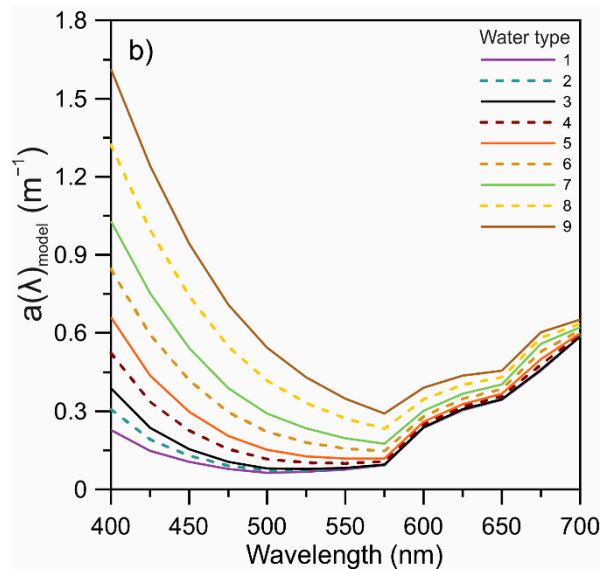
Figure 5. Intermediate water types (dashed lines), added to the original Jerlov coastal water types.

Figure 6 illustrates the classification procedure into Jerlov water types. Four stations were selected as examples, which were contrasted according to a goodness-of-fit test based on a least-squares fitting method [35]. In each panel of Figure 6, $a(\lambda)_{in\ situ}$ of the selected stations and $a(\lambda)_{model}$ of different types of water (II, 4, 6, and 8) are displayed with the respective χ^2_{Cal} values that represent the integration of the square distances between $a(\lambda)_{in\ situ}$ and $a(\lambda)_{model}$. The water type for which χ^2_{Cal} is minimum was selected (if the value was zero, this would imply a perfect fit, i.e., $a(\lambda)_{in\ situ}$ is equal to $a(\lambda)_{model}$). In Figure 6a, station D05 presented a $\chi^2_{Cal} = 1.46$, this being the smallest value relative to all other stations,

indicating that it must be classified as a type-II water. In Figure 6b, the lowest χ^2_{Cal} corresponded to station B06, so it was classified as type 4. For water type 6, which is exemplified in Figure 6c, station 247 showed the lowest χ^2_{Cal}. When stations were contrasted with water type 8 (Figure 6d), station 071 had the lowest χ^2_{Cal}.
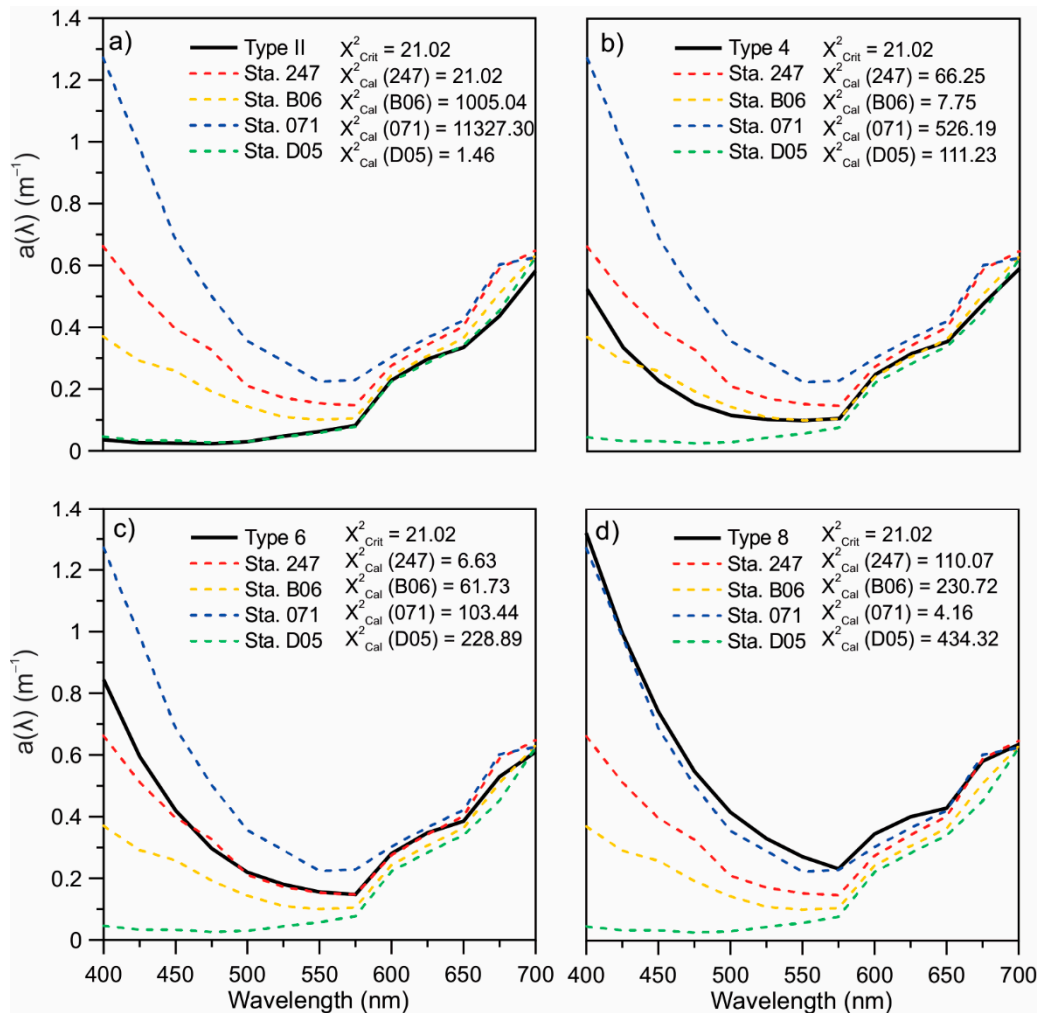
Figure 6. Least-squares fitting method for four selected stations. The black line indicates $a(\lambda)_{model}$ values for the different water types; the dotted line, $a(\lambda)_{in\ situ}$ for stations. χ^2_{Crit} marks the maximum allowable tolerance for the fit. (**a**) Example of the fit for type II, where station D05 gave the best fit; (**b**) example of the fit for type 4, where station B06 gave the best fit; (**c**) example of the fit for type 6, where station 247 gave the best fit; (**d**) example of the fit for type 8, where station 071 gave the best fit.

The classification into Jerlov water types yielded the results shown in Table 3, with 48 oceanic stations (i.e., types I–III) and 65 coastal stations (i.e., types 1–9). No water type 3 was found in the reduced data set. Figure 4b shows that the clear water case ($Z_{SD} \geq 5.37$ m.) comprises all the ocean groups (I, IA, IB, II, III) and the most transparent coastal groups (1–4), with $K_{d\ in\ situ}$ values of less than 0.2 m^{-1}. The turbid-water case ($Z_{SD} < 2.20$ m) included the most turbid coastal waters (5–9), with $K_{d\ in\ situ}$ values above 0.4 m^{-1}. Additionally, the transition zone shows the interaction between groups 4, 5, 6, and 7, comprising stations ranging from clear (4) to turbid (5–7) waters, where some stations (for example, group 6) show turbid waters while other stations in the same group belong to the transition zone. Figure 4b also shows an overlap of water types for a given Z_{SD} in the group of oceanic waters. This also occurs for the group of clear coastal waters that includes types 1, 2, and 4, with an overlap between the few type 2 and type 1 cases. In addition, if data representing type 3 were

available, these would presumably overlap with type 4. Finally, and consistent with the above, the group of turbid coastal waters (types 5–9) exhibits an overlap between optical types. These results show that the relationship between Z_{SD} (or deduced K_d (PAR)) and water type, as determined from a (λ), is not unique (i.e., a given Z_{SD} or range of Z_{SD} values may be associated to different water types), thus limiting the ability to derive specific inherent optical properties from Z_{SD} as the only variable, even in statistic terms. This is hardly surprising, since K_d (PAR) is non-spectral and depends not only on a (λ) but also on spectral particulate backscattering [23]. Note that the model proposed by Solonenko and Mobley [30] to associate the inherent optical properties with Jerlov water type does not consider the contribution of non-phytoplankton particulate material, which comprises phytoplankton detritus plus other organic and mineral particles. They argue that it is sufficient to model absorption as a function of chlorophyll and CDOM in both Case-1 and Case-2 waters, and even for the most turbid waters. In areas highly influenced by non-phytoplankton particulate matter (e.g., mineral sources), however, the absorption of these components likely influences the association of the inherent optical properties with water type. Therefore, Jerlov's classification needs to be adapted to account for such scenarios in turbid coastal environments, including coastal lagoons, estuaries, and river mouths.

Table 3. Number of observations (N) classified into a Jerlov water type for the 113 stations with a.

Descriptors	Oceanic					Coastal								
Water Type	I	IA	IB	II	III	1	2	3	4	5	6	7	8	9
N	2	4	4	8	26	21	2	-	6	5	7	14	6	8

Considering the 113 data that were optically classified into the different Jerlov water types (Table 3), a model might theoretically be derived for each type of water; however, the number of observations for some optical types is small. It was therefore decided to split the 113 data into two groups, oceanic and coastal, and work only with those types of water including more than 10 observations, aiming of derive a specific model for each. For estimating the models, observations for each type of water (oceanic, coastal, III, 1, and 7) were randomly sorted into two groups (50% for modeling and 50% for validation purposes). Once the models were obtained, these were applied to the dataset to validate them, and contrasted against model *c*, which is the best model from the previous analyses. These comparisons are shown in Table 4. In this case, MPI (Equation (12)) was not suitable due to the small number of observations; thus, the best model was the one showing the lowest MAE (Equation (9)) and RMSD (Equation (10)) values, and the BIAS (Equation (11)) value closest to zero.

Table 4. Evaluation of the $K_{d\,in\,situ}$ versus a specific model by water type and model *c*. The bold show the best results.

Water Type	Model	Equation	MAE	RMSD	BIAS
Oceanic group	Model *c*	Equations (15)–(17)	**0.016**	**0.018**	**0.016**
	Model oceanic	$K_d = 0.089/(Z_{SD})^{0.518}$	0.550	0.020	0.055
Coastal group	Model *c*	Equations (15)–(17)	**0.149**	**0.260**	**0.037**
	Model coastal	$K_d = 1.79/(Z_{SD})^{0.978}$	0.346	0.469	−0.343
III	Model *c*	Equations (15)–(17)	**0.011**	**0.009**	**0.011**
	Model III	$K_d = 0.37/(Z_{SD})^{0.673}$	0.027	0.010	0.027
1	Model *c*	Equations (15)–(17)	**0.021**	**0.027**	**0.016**
	Model 1	$K_d = 0.66/(Z_{SD})^{0.784}$	0.027	0.027	0.025
7	Model *c*	Equations (15)–(17)	**0.051**	**0.053**	**−0.032**
	Model 7	$K_d = 0.95/(Z_{SD})^{0.667}$	0.105	0.074	0.105

Model *c* is the best fit in all cases because this model contemplates three intervals of Z_{SD}; also, in each interval, this model makes an approximation based on a nonlinear model (Equation (2)). Consequently, this is an adaptive model that estimates the best combination regardless of the optical type of water being analyzed. In this regard, we consider that the development of model *c* simplifies of the estimate K_d based on Z_{SD} regardless of the type of water. Model *c* can be applied to different

marine optical conditions; however, it is advisable to continue obtaining measurements of Jerlov's water types to determine the contribution of each individual component present in seawater to the calculation of K_d.

Continuing with the simultaneous measurement of Z_{SD} and K_d with an irradiance-meter will facilitate obtaining better coefficients in each equation of the adaptive model. Additional measurements should be performed, especially in turbid coastal waters, including coastal lagoons, estuaries, and river mouths.

There is the need to implement marine monitoring systems to detect changes in ecosystems. Water turbidity may provide information on environmental alterations, and the monitoring thereof based on estimations of K_d (PAR) from Z_{SD} using empirical models such as model c is sufficiently accurate and cost-effective. The potential sources of error in these estimates, which were analyzed by Preisendorfer [10], should however be kept in mind to ensure that the results obtained reflect the true variability across water parcels.

4. Conclusions

K_d is a valuable tool for monitoring both spatio-temporal changes and long-term trends in the water column. The estimation of K_d based on Z_{SD} measurements is a low-cost methodology that can be used systematically in oceanographic campaigns due to its easy application/implementation. However, to ensure consistent results, care must be taken regarding the methodology to measure Z_{SD}. The classical approaches for calculating K_d from Z_{SD}, based on a single OD_{SD} value, do not accurately represent the broad range of optical conditions that occur in the marine environment. The adaptive model proposed in this work represents the optical diversity under various conditions, ranging from clear ocean waters to highly turbid coastal waters. It provides continuity across Z_{SD} and, importantly, improves K_d retrieval under clear, turbid, and transition scenarios. This model calculates K_d considering three ranges of Z_{SD} values, as described by the following equations:

$$
\begin{aligned}
&\text{If } Z_{SD} < 2.20 \text{ m, then } K_{d\,model\,c} = \frac{1.16}{(Z_{SD})^{0.62}} \\
&\text{If } 2.20 \text{ m} \leq Z_{SD} < 5.37 \text{ m, then} \\
K_{d\,model\,c} =\ &\exp\left((0.15 - logZ_{SD} \times 0.62) \times \frac{1.68 - logZ_{SD}}{0.89} + (-0.48 - logZ_{SD} \times 0.72) \times \frac{logZ_{SD} - 0.79}{0.89} \right) \\
&\text{If } Z_{SD} \geq 5.37 \text{ m, then } K_{d\,model\,c} = \frac{0.62}{(Z_{SD})^{0.72}}
\end{aligned}
\tag{18}
$$

The marine optical water classification is a potential approach in studies addressing the relationship between K_d (PAR) and optical characteristics. However, our classification of 113 stations with absorption data into Jerlov water types indicated that no unique water type could be related to a given Z_{SD} or K_d (PAR), thus making it difficult to use Z_{SD} measurements to infer the optical properties and chlorophyll concentrations of particular water types. This is likely due to the fact that K_d (PAR) is the overall result of the variability in both the quantity and type of material (dissolved or particulate matter) present in the water column. In addition, it should be noted that different optical types may occur at the same time in the water column, so that K_d (PAR) may result from the combination of different water types. Given this complexity, data derived from satellite observations are promising and this field of research should be further refined in the future.

Author Contributions: Conceptualization, A.C.-R., E.S.-d.-Á., A.G.-S., R.F., M.-T.S.-F., J.L.-C., L.S.-V. and L.E.-P.; Data curation, A.C.-R. and E.S.-d.-Á.; Formal analysis, A.C.-R., E.S.-d.-Á., R.F. and J.T.; Funding acquisition, E.S.-d.-Á., A.G.-S., R.F. and L.S.-V.; Investigation, A.C.-R., E.S.-d.-Á., A.G.-S., R.F., M.-T.S.-F., J.T., J.L.-C., L.S.-V. and L.E.-P.; Methodology, A.C.-R., E.S.-d.-Á., A.G.-S., R.F., M.-T.S.-F., J.T., J.L.-C., L.S.-V. and L.E.-P.; Project administration, E.S.-d.-Á., A.G.-S., R.F. and L.S.-V.; Resources, E.S.-d.-Á., A.G.-S. and R.F.; Supervision, A.C.-R., E.S.-d.-Á., A.G.-S., R.F., M.-T.S.-F., J.T., J.L.-C., L.S.-V. and L.E.-P.; Validation, A.C.-R., E.S.-d.-Á., R.F. and J.T.; Visualization, A.C.-R., E.S.-d.-Á., R.F. and J.T.; Writing—original draft, A.C.-R., E.S.-d.-Á., A.G.-S., R.F., M.-T.S.-F.

References

1. Kirk, J.T.O. *Light and Photosynthesis in Aquatic Ecosystems*, 3rd ed.; Cambridge University Press: Cambridge, UK, 2011; p. 649.

2. Frouin, R.; Ramon, D.; Boss, E.; Jolivet, D.; Compiègne, M.; Tan, J.; Bouma, H.; Jackso, T.; Franz, B.; Platt, T.; et al. Satellite Radiation Products for Ocean Biology and Biogeochemistry: Needs, State-of-the-Art, Gaps, Development Priorities, and Opportunities. *Front. Mar. Sci.* **2018**, *5*, 3. [CrossRef]

3. Platt, T.; Denman, K.L.; Jassby, A.D. *Modeling the Productivity of Phytoplankton, in the Sea: Ideas and Observations on Progress in the Study of the Seas*; Goldberg, E.D., Ed.; John Wiley: New York, NY, USA, 1977; pp. 807–856.

4. Falkowski, P.G.; Raven, J.A. *Aquatic Photosynthesis*; Blackwell Science: Malden, MA, USA, 1997; p. 375.

5. Antoine, D.; Babin, M.; Berthon, J.; Bricaud, A.; Gentili, B.; Loisel, H.; Maritorena, S.; Stramski, D. Shedding Light on the Sea: André Morel's Legacy to Optical Oceanography. *Annu. Rev. Mar. Sci.* **2014**, *6*, 1–21. [CrossRef] [PubMed]

6. Secchi, A. Schreiben des Herrn Prof. Secchi, Directors der Sternwarte des Collegio Romano, an den Herausgeber. *Astron. Nachr.* **1866**, *68*, 63. [CrossRef]

7. Wernard, M.R. On the history of the Secchi Disk. *J. Eur. Opt. Soc.-Rapid* **2010**, *5*, 100135. [CrossRef]

8. Davies-Colley, R.J.; Vant, W.N.; Smith, D.G. *Colour and Clarity of Natural Waters. Science and Management of Optical Water Quality*; Ellis-Horwood: New York, NY, USA, 1993; p. 310.

9. Poole, H.H.; Atkins, W.R.G. Photo-Electric Measurements of Submarine Illumination throughout the Year. *J. Mar. Biol Assoc. UK* **1929**, *16*, 297–324. [CrossRef]

10. Preisendorfer, R.W. Secchi disk science: Visual optics of natural waters. *Limnol. Oceanogr.* **1986**, *31*, 909–926. [CrossRef]

11. Lund-Hansen, L.C. Diffuse Attenuation Coefficients Kd(PAR) at the Estuarine North Sea–Baltic Sea Transition: Time-Series, Partitioning, Absorption, and Scattering. *Estua Coast. Shelf Sci.* **2004**, *61*, 251–259. [CrossRef]

12. Pope, R.M.; Fry, E.S. Absorption Spectrum (380–700 nm) of Pure Water. II. Integrating Cavity Measurements. *Appl. Opt.* **1997**, *36*, 8710–8723. [CrossRef]

13. Prieur, L.; Sathyendranath, S. An Optical Classification of Coastal and Oceanic Waters Based on the Specific Spectral Absorption Curves of Phytoplankton Pigments, Dissolved Organic Matter, and Other Particulate Materials. *Limnol. Oceanogr.* **1981**, *26*, 671–689. [CrossRef]

14. Santamaría-del-Ángel, E.; Millán-Núñez, R.; González-Silvera, A.; Cajal-Medrano, R. *Producción Primaria Fitoplanctónicas. En Manuales del cuerpo Académico de Ecología del Fitoplancton de la Facultad de Ciencias Marinas de la Universidad Autónoma de Baja California*; Series White Papers POPEYE 41 p; Universidad Autónoma de Baja California, Facultad de Ciencias Marinas: Ensenada, Mexico, 2005. [CrossRef]

15. Holmes, R.W. The Secchi disk in turbid coastal waters. *Limnol. Oceanogr.* **1970**, *15*, 688–694. [CrossRef]

16. Megard, R.O.; Berman, T. Effects of algae on the Secchi transparency of the southeastern Mediterranean Sea. *Limnol. Oceanogr.* **1989**, *34*, 1640–1655. [CrossRef]

17. Montes-Hugo, M.A.; Álvarez-Borrego, S. Empirical relations to estimate PAR attenuation in San Quintín Bay, using Secchi depth and sighting range. *Cienc Mar.* **2005**, *31*, 685–695. [CrossRef]

18. Lee, Z.; Shang, S.; Du, K.; Wei, J. Resolving the Long-Standing Puzzles about the Observed Secchi Depth Relationships. *Limnol. Oceanogr.* **2018**, *63*, 2321–2336. [CrossRef]

19. Harvey, E.T.; Walve, J.; Andersson, A.; Karlson, B.; Kratzer, S. The effect of optical properties on Secchi depth and implications for eutrophication management. *Front. Mar. Sci.* **2019**, *5*, 496. [CrossRef]

20. Steinmetz, H.; Staudinger, M.; Balch, W.M. Analyzing the Effects of Coccolithophore Concentration on the Relationship between Vertical Absorption Coefficient and Secchi Disk Depth. Student Showcase. 2019. Available online: https://scholarworks.umass.edu/sustainableumass_studentshowcase/26 (accessed on 10 June 2020).

21. Gallegos, C.L.; Werdell, P.J.; McClain, C.R. Longterm changes in light scattering in Chesapeake Bay inferred from Secchi depth, light attenuation, and remote sensing measurements. *J. Geophys. Res.* **2011**, *116*, C00H08. [CrossRef]

22. Barbosa, A.; Domingues, R. Effects of Nutrient and Light Enrichment on Phytoplankton Growth. In *Practical Experiments Guide for Ecohydrology*; Chícharo, L., Wagner, I., Chicharo, M., Lapinska, M., Zalewski, M., Eds.; UNESCO: Venice, Italy, 2009; pp. 27–30.

23. Lee, Z.; Shang, S.; Hu, C.; Du, K.; Weidemann, A.; Hou, W.; Lin, J.; Lin, G. Secchi disk depth: A new theory and mechanistic model for underwater visibility. *Remote Sens. Environ.* **2015**, *169*, 139–149. [CrossRef]

24. IOCCG. *Remote Sensing of Inherent Optical Properties: Fundamentals, Tests of Algorithms, and Applications. In Reports of the International Ocean Colour Coordinating Group No. 5*; Lee, Z.P., Ed.; IOCCG: Dartmouth, NS, Canada, 2006; p. 126.

25. Mobley, C.D.; Sundman, L.K. *HydroLight 5.2 User's Guide*; Sequoia Scientific: Seattle, WA, USA, 2013.

26. Padial, A.A.; Thomaz, S.M. Prediction of the light attenuation coefficient through the Secchi disk depth: Empirical modeling in two large Neotropical ecosystems. *Limnology* **2008**, *9*, 143–151. [CrossRef]

27. Ficek, D.; Zapadka, T. Variability of bio-optical parameters in Lake Jasień Północny and Lake Jasień Południowy. *Limnol. Rev.* **2010**, *10*, 67–76. [CrossRef]

28. Zhang, Y.; Liu, X.; Yin, Y.; Wang, M.; Qin, B. Predicting the light attenuation coefficient through Secchi disk depth and beam attenuation coefficient in a large, shallow, freshwater lake. *Hydrobiologia* **2012**, *693*, 29–37. [CrossRef]

29. Jerlov, N.G. *Optical Oceanography*; American Elsevier Publishing Company Incorporation: New York, NY, USA, 1968; p. 194.

30. Solonenko, M.G.; Mobley, C.D. Inherent optical properties of Jerlov water types. *Appl. Opt.* **2015**, *54*, 5392–5401. [CrossRef]

31. Tara Oceans Consortium, Coordinators; Tara Oceans Expedition. *Environmental Context of All Samples from the Tara Oceans Expedition (2009–2013), about Mesoscale Features*; PANGAEA: Bremerhaven, Germany, 2016. [CrossRef]

32. Werdell, P.J.; Bailey, S.W. An improved bio-optical data set for ocean color algorithm development and satellite data product validation. *Remote Sens. Environ.* **2005**, *98*, 122–140. [CrossRef]

33. Steyerberg, E.W. Validation of Prediction Models. In *Clinical Prediction Models. Statistics for Biology and Health*, 2nd ed.; Springer: Cham, Germany, 2019; pp. 329–344.

34. IOCCG. *Synergy between Ocean Colour and Biogeochemical/Ecosystem Models 2020*; IOCCG Report Series, No. 19; Dutkiewicz, S., Ed.; International Ocean Colour Coordinating Group: Dartmouth, NS, Canada, 2020. [CrossRef]

35. Xu, W.; Chen, W.; Liang, Y. Feasibility Study on the Least Square Method for Fitting Non-Gaussian Noise Data. *Phys. A Stat. Mech. Appl.* **2017**, *492*, 1917–1930. [CrossRef]

36. Ocean Color Data. Available online: https://oceandata.sci.gsfc.nasa.gov/ (accessed on 5 July 2020).

37. Kahru, M.; Kudela, R.M.; Anderson, C.R.; Mitchell, B.G. Optimized merger of ocean chlorophyll algorithms of MODIS-Aqua and VIIRS. *IEEE Geosci. Remote Sens.* **2015**, *12*, 11. [CrossRef]

38. Kahru, M.; Di Lorenzo, E.; Manzano-Sarabia, M.; Mitchell, B.G. Spatial and temporal statistics of sea surface temperature and chlorophyll fronts in the California Current. *J. Plankton Res.* **2012**, *34*, 749–760. [CrossRef]

39. Wilcoxon, F. Individual Comparisons by Ranking Methods. *Biom. Bull.* **1945**, *1*, 80–83. [CrossRef]

40. Wilcoxon, F.; Katti, S.K.; Wilcox, R.A. *Critical Values and Probability Levels for the Wilcoxon Rank Sum Test and the Signed Rank Test*; American Cyanamid Co., & Lederle Lab.: Pearl River, NY, USA, 1963.

41. Wilcoxon, F.; Katti, S.K.; Wilcox, R.A. Critical Values and Probability Levels for the Wilcoxon Rank Sum Test and the Wilcoxon Signed Rank Test. In *Selected Tables in Mathematical Statistics*; Amer Mathematical Society: Providence, RI, USA, 1970; Volume 1, pp. 171–259.

42. Mitchell, B.G.; Bricaud, A.; Carder, K.; Cleveland, J.; Ferrari, G.M.; Gould, R.; Kahru, M.; Kishino, M.; Maske, H.; Moisan, T.; et al. Determination of Spectral Absorption Coefficients of Particles, Dissolved Material and Phytoplankton for Discrete Water Samples. In *Ocean Optics Protocols for Satellite Ocean Color Sensor Validation*; Revision 2; Fargion, G.S., Mueller, J.L., McClain, C.R., Eds.; Goddard Space Flight Space Center: Greenbelt, MD, USA, 2000; pp. 125–153.

43. Mueller, J.L.; Austin, R.W. *Ocean Optics Protocols for SeaWIFS Validation*; Revision 1; SeaWiFS Technical Report Series; Hooker, S.B., Firestone, E.R., Acker, J.G., Mueller, J.L., Austin, R.W., Eds.; Goddard Space Flight Space Center: Greenbelt, MD, USA, 1995; p. 25.

44. Zar, J.H. *Biostatistical Analysis*, 5th ed.; Prentice-Hall: New Jersey, NJ, USA, 2010; p. 944.

45. Koenings, J.P.; Edmundson, J.A. Secchi disk and photometer estimates of light regimes in Alaskan lakes: Effects of yellow color and turbidity. *Limnol. Oceanogr.* **1991**, *36*, 91–105. [CrossRef]

46. Lugo-Fernández, A.; Gravois, M.; Montgomery, T. Analysis of Secchi depths and light attenuation coefficients in the Louisiana-Texas shelf, northern Gulf of Mexico. *Gulf Mex. Sci.* **2008**, *26*, 14–27. [CrossRef]

47. Santamaría-del-Ángel, E.; Millán-Núñez, R.; Soto, I.; González-Silvera, A.; Wolny, J.; Cerdeira-Estrada, S.; Cajal-Medrano, R.; Muller-Karger, F.; Padilla-Rosas, Y.X.S.; Mercado-Santana, A.; et al. Phytoplankton Blooms: New Initiative Using Marine Optics as a Basis for Monitoring Programs. In *Coastal Ecosystems: Experiences and Recommendations for Environmental Monitoring Programs*; Nova Science Publisher: New York, NY, USA, 2015; Chapter 4.

48. Aguilar-Maldonado, J.A.; Santamaría-del-Ángel, E.; González-Silvera, A.; Cervantes-Rosas, O.; López, L.M.; Gutiérrez-Magness, A.; Cerdeira-Estrada, S.; Sebastiá-Frasquet, M.T. Identification of Phytoplankton Blooms under the Index of Inherent Optical Properties (IOP Index) in Optically Complex Waters. *Water* **2018**, *10*, 129. [CrossRef]

49. Austin, R.W.; Petzold, T.J. The Determination of the Diffuse Attenuation Coefficient of Sea Water Using the Coastal Zone Color Scanner. In *Oceanography from Space*; Springer: Boston, MA, USA, 1981; pp. 239–256.

50. Hicks, B.J.; Stichbury, G.A.; Brabyn, L.K.; Allan, M.G.; Ashraf, S. Hindcasting water clarity from Landsat satellite images of unmonitored shallow lakes in the Waikato region, New Zealand. *Environ. Monit. Assess.* **2013**, *185*, 7245–7261. [CrossRef]

51. Butt, M.J.; Nazeer, M. Landsat ETM+ Secchi Disc Transparency (SDT) retrievals for Rawal Lake, Pakistan. *Adv. Space Res.* **2015**, *56*, 1428–1440. [CrossRef]

52. Rodrigues, T.; Alcântara, E.; Watanabe, F.; Imai, N. Retrieval of Secchi disk depth from a reservoir using a semi-analytical scheme. *Remote Sens. Environ.* **2017**, *198*, 213–228. [CrossRef]

53. Leite, H.R.; de Oliveira, F.A.; Drago, D.; Muraro, A.; Teixeira, L.F.; Hainosz, F.S.; Prochnow, R.M.; Quicu, S.T.; Nascimento, C. Natural effects on remote sensing of water quality parameters data: A case study on available algorithms at the Jupia Reservoir, Brazil. In *Remote Sensing of the Ocean, Sea Ice, Coastal Waters, and Large Water Regions*; International Society for Optics and Photonics: Washington, DC, USA, 2019; Volume 11150, p. 1115006.

54. Nouchi, V.; Kutser, T.; Wüest, A.; Müller, B.; Odermatt, D.; Baracchini, T.; Bouffard, D. Resolving biogeochemical processes in lakes using remote sensing. *Aquat. Sci.* **2019**, *81*, 27. [CrossRef]

55. Kim, S.H.; Yang, C.S.; Ouchi, K. Validation of the semi-analytical algorithm for estimating vertical underwater visibility using MODIS data in the waters around Korea. *Korean J. Remote Sens.* **2013**, *29*, 601–610. [CrossRef]

56. Tyler, J.E. The Secchi Disk. *Limnol. Oceanogr.* **1968**, *13*, 1–6. [CrossRef]

57. Doron, M.; Babin, M.; Mangin, A.; Hembise, O. Estimation of light concentration, and horizontal and vertical visibility in oceanic and coastal waters from surface reflectance. *J. Geophys. Res.* **2007**, *112*, C06003. [CrossRef]

58. Doron, M.; Babin, M.; Hembise, O.; Mangin, A.; Garnesson, P. Ocean transparency from space: Validation of algorithm estimating Secchi depth using MERIS, MODIS and SeaWiFS data. *Remote Sens. Environ.* **2011**, *115*, 2986–3001. [CrossRef]

59. Betancur-Turizo, S.P.; González-Silvera, A.G.; Santamaría-Del-Ángel, E.; Millán-Núñez, R.; Millán-Núñez, E.; García-Nava, H.; Godínez, V.M.; Sánchez-Velasco, L. Variability in the Light Absorption Coefficient by Phytoplankton, Non-Algal Particles and Colored Dissolved Organic Matter in the Northern Gulf of California. *Open J. Mar. Sci.* **2018**, *8*, 20–37. [CrossRef]

60. Jiang, D.; Matsushita, B.; Setiawan, F.; Vundo, A. An improved algorithm for estimating the Secchi disk depth from remote sensing data based on the new underwater visibility theory. *ISPRS J. Photogramm.* **2019**, *152*, 13–23. [CrossRef]

61. Liu, Y.; Xiao, C.; Li, J.; Zhang, F.; Wang, S. Secchi Disk Depth Estimation from China's New Generation of GF-5 Hyperspectral Observations Using a Semi-Analytical Scheme. *Remote Sens.* **2020**, *12*, 1849. [CrossRef]

62. Arabi, B.; Salama, M.S.; Pitarch, J.; Verhoef, W. Integration of in-situ and multi-sensor satellite observations for long-term water quality monitoring in coastal areas. *Remote Sens. Environ.* **2020**, *239*, 111632. [CrossRef]

63. Djavidnia, S.; Ott, M.; Seeyave, S. (Eds.) *Oceans and Society: Blue Planet*; Cambridge Scholars Publishing: Newcastle upon Tyne, UK, 2014.